Unveiling the effect of confinement on reinforcement-concrete bond behavior using discrete lattice model

Liu, Xun; Gu, Dawei; Pan, Jinlong; Luković, Mladena

DOI
10.1016/j.engfracmech.2025.111510

Publication date
2025

Document Version
Final published version

Published in
Engineering Fracture Mechanics

Engineering Fracture Mechanics 328 (2025) 111510

Contents lists available at ScienceDirect

Engineering Fracture Mechanics

journal homepage: www.elsevier.com/locate/engfracmech

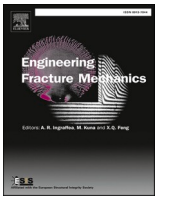

Unveiling the effect of confinement on reinforcement-concrete bond behavior using discrete lattice model

Xun Liu [a], Dawei Gu [a,b,*], Jinlong Pan [a], Mladena Luković [b]

[a] School of Civil Engineering, Southeast University, Nanjing 211189, China
[b] Faculty of Civil Engineering and Geosciences, Delft University of Technology, Delft 2600 AA, Netherlands

ARTICLE INFO

Keywords:
Reinforcement-concrete bond
Confinement
Lattice model
Lap splices
Failure mechanism

ABSTRACT

Understanding the bond behavior between reinforcement and concrete under varying confinement conditions is essential for the design and performance assessment of reinforced concrete structures. This study employs a discrete lattice model to investigate the reinforcement-concrete bond mechanism, focusing on crack propagation, fracture processes, and stress distribution. Experimental data involving lap-spliced reinforcement bond test under different confinement conditions serve as benchmarks. In the model, concrete, reinforcement, and their interface are discretized into beam elements, while the interface properties remain constant and independent of confinement conditions. A key finding is that generating the lattice mesh through the Delaunay triangulation scheme enables the model to reproduce realistic strut-cracking patterns and conical stress transfer phenomena, thereby capturing stirrup-induced passive confinement effects without modifying interface properties. The results clarify the role of stirrup confinement in restricting concrete dilatancy and bond splitting, while bond failure is shown to depend on concrete fracture under weak confinement and on interface failure only under strong confinement. Overall, this study not only validates the discrete lattice approach for reinforced concrete bond modeling but also provides deeper insights into lap-splice failure mechanisms, offering a robust framework for structural assessment and design.

1. Introduction

The bond between reinforcement and concrete is crucial for the load-carrying capacity, deformational capacity, crack control and durability of reinforced concrete structures [1–3]. A set of factors, such as concrete cover thickness, reinforcement diameter, rib spacing, confinement and boundary conditions, and concrete and reinforcement mechanical properties, significantly influence the bond behavior between reinforcement and concrete [4,5]. Therefore, understanding and evaluating the bond behavior, particularly its failure mechanism, is of great significance but is highly complex.

To date, extensive experimental research has been conducted to investigate the reinforcement-concrete bond behavior, in which the pull-out test of single bar embedded in concrete [6–8] and the four-point bending test of concrete beam reinforced with lap-spliced bars [9–12] are the two widely used testing schemes. Compared to the beam testing scheme, the pull-out test is more direct and easier to conduct due to the simpler specimen fabrication and loading. However, it tends to over-estimate the bond strength attributing to the unrealistic strong confinement by the rigid supports [13]. Additionally, in pull-out tests, concrete is subjected to compression to induce

* Corresponding author.
E-mail address: dwgu@seu.edu.cn (D. Gu).

https://doi.org/10.1016/j.engfracmech.2025.111510
Received 21 May 2025; Received in revised form 21 August 2025; Accepted 24 August 2025
Available online 29 August 2025

Nomenclature

A_r	cross-sectional area of reinforcement;
c	cover thickness of concrete;
c_0	clear distance between the ribs on bars;
D	diameter of reinforcement;
d_b	diameter of lap-spliced reinforcement;
E	elastic modulus of concrete elements;
E_n	elastic modulus of interface elements for nth segment;
$\mathrm{E}\left[\frac{K_{n,\text{non-aligned}}}{K_{n,\text{aligned}}}\right]$	the expectation of bond stiffness ratio between reinforcement with aligned and non-aligned interface elements;
$\mathrm{E}\left[\frac{u_{n,\text{non-aligned}}}{u_{n,\text{aligned}}}\right]$	the expectation of the bond strength ratio between reinforcement with aligned and non-aligned interface elements;
f_c	compressive strength of concrete elements;
f'_c	cylindrical concrete compression strength;
f_n	interface element strength for nth segment;
f_t	tensile strength of concrete elements;
G	shear modulus of concrete elements;
G_n	shear modulus of interface element for nth segment;
L_v	voxel size;
L_s	sub-voxel size;
l_s	splice length;
s_I	slip at the onset of the peak bond stress plateau in the pull-out failure envelope;
s_{II}	slip at the endpoint of the peak bond stress plateau in the pull-out failure envelope;
s_{III}	slip at the onset of the residual bond stress plateau in the pull-out failure envelope;
u	average bond stress;
u_f	residual bond strength in pull-out failure envelope;
u_m	peak bond strength in pull-out failure envelope;
u_{max}	peak bond strength of lap splice;
$u_{max,exp}$	tested bond strength;
$u_{max,pre}$	predicted bond strength;
R	radius of concrete elements;
r	radius of the interface element;
ν	Poisson's ratio of the interface element.

pull-out failure, whereas in actual structures, both the reinforcement and the surrounding concrete are typically under tension. Instead, ACI committee 408 [14] recommends the beam test for investigating the bond behavior of reinforcement embedded in concrete, because the beam test more accurately reflects the stress state of concrete in real structures [15,16]. Through beam tests, and by using newly developed measuring technologies, a range of reinforcement-concrete bond deterioration phenomena can be directly captured. For example, the local strain and shear stress transfer along the full-length of reinforcement can be assessed by distributed fiber optical sensing [17], and the surface crack evolution can be detected by the digital image correlation (DIC) technique [18]. However, significant challenges remain in monitoring the development of internal cracks within in-situ large-scale specimens during loading, leading to a limited understanding of the underlying failure mechanisms.

As the experimental study can be limited to observing cracking behavior on the surface of structures, the numerical analysis often acts as an essential complementary approach for uncovering the internal fracture process and gaining a deeper understanding of bond failure mechanisms. Using the finite element method (FEM), Jakubovskis et al. [19] explicitly modelled the ribs on deformed bar, which accurately predicted the bond stress distribution and the formation of microcracks in the surrounding concrete. However, the very fine element mesh required around the ribs resulted in high computational costs, and the numerical results were highly sensitive to the geometric parameters of simplified rib shapes. Instead, Ooi et al. [20] employed a type of cohesive interface element to model the reinforcement-concrete bond, whereas the local remeshing of concrete elements was necessary for simulating the propagation of multiple cohesive cracks within reinforced concrete. Additionally, modelling the reinforcement using one-dimensional truss elements and representing the reinforcement-concrete bond with spring elements or embedded bond-slip relationships is a more common approach for simulating the structural behavior of reinforced concrete [21–23]. The properties of these spring elements or embedded bond are defined by phenomenological reinforcement-concrete bond-slip laws, which are often related to the structural parameters such as concrete cover thickness, confinement conditions and loading schemes. However, such modeling approach fails to capture fundamental bond failure mechanisms, such as concrete cover splitting caused by the radial component of the bond force [24] and fails to predict bond behavior under changed boundary or confinement conditions.

Compared to continuum models, discrete element models offer advantages in simulating the fracture behavior of concrete structures. Among various models, the lattice discrete particle model (LDPM) has been proven to be one of the most appealing

computational tools. In LDPM, irregular meshing methodologies (random lattice mesh or polygonal/polyhedral assemblage cells interacting through lattice struts) can be applied to represent the nonlinear behavior of concrete under a variety of loading conditions [25]. This approach is capable of accurately predicting the ultimate flexural behavior of RC beams with a wide range of main and secondary reinforcements but demands extremely large computational effort [26]. As an alternative to overcome this drawback, the rigid body spring model (RBSM) discretizes concrete into rigid bodies and represents reinforcement by beam elements [27]. The bond between reinforcement and concrete is modelled using spring elements, with their properties defined by the user-defined bond-slip relationship. This approach can effectively evaluate changes in internal cracking and stress distribution due to variations in concrete cover thickness and reinforcement diameter [10,28,29].

Unlike RBSM, the Delft lattice model discretizes the continuum into randomly distributed beam elements, with the cracking process modelled as the step-by-step removal of elements using a sequential algorithm [30]. It has been widely applied to simulate the fracture behavior of quasi-brittle materials like cement and concrete at the micro- and *meso*-scale [30–34]. However, in its conventional form, the Delft lattice model employs purely linear elastic beam elements to represent all material phases. This simplification restricts its capability to capture the plastic deformation of steel reinforcement and provides no straightforward means of defining the reinforcement-concrete interface, thereby limiting its application to reinforced concrete structures. To overcome this challenge, recent pilot studies by the authors [35–37] proposed an extended framework in which both the reinforcement and the reinforcement-concrete interface are also modeled by beam elements, with their nonlinear behavior described through multi-segmental linear constitutive laws. In this formulation, elements are not immediately removed once the failure criterion is reached; instead, they are updated to the next segment of the piecewise linear law, and this process continues until ultimate failure occurs. This strategy has proven effective and has demonstrated strong potential for simulating the fracture behavior of reinforced concrete members [35–37].

Having addressed the challenges related to element type and constitutive formulation, the critical step toward achieving cross-scale simulation of reinforced concrete structures lies in the accurate representation of reinforcement-concrete interface behavior. To this end, two fundamental questions must be resolved: (1) how should the properties of reinforcement-concrete interface elements in a beam-type lattice model be determined? and (2) since the majority of reinforced concrete members incorporate stirrups or other forms of transverse reinforcement, can the discrete lattice model still reliably capture the effect of confinement on bond behavior under such conditions? Only when both issues are satisfactorily addressed can the discrete lattice model be considered a robust framework for extending simulations from the fracture behavior of cementitious materials at the *meso*-scale to the mechanical response of reinforced concrete structures at the structural scale.

With respect to the first issue, it should be noted that in the beam-type lattice model all phases (including the reinforcement-concrete interface) are represented by beam elements. The challenge, therefore, is to determine the attributes of these interface elements (radius, multi-segment elastic modulus, shear modulus, tensile and compressive strength) such that they reproduce a target bond stress-slip relationship. A straightforward but inefficient approach is trial-and-error calibration [35]. However, because bond stress-slip relationships are inherently nonlinear, iterative calibration becomes both time-consuming and unreliable. To overcome this limitation, Gu et al. [36] developed a calibration-free stochastic method that, given a bond stress-slip curve, can directly derive the corresponding interface element parameters. This method was validated through numerical simulations of pull-out tests, confirming its feasibility.

Building on this foundation, the present study addresses the second issue by performing discrete lattice simulations of reinforcement-concrete bond under varying confinement conditions. Benchmark data were taken from the lap-splice bond tests conducted by Harajli et al. [12], where classical four-point bending beam tests were carried out to examine the influence of stirrup confinement and concrete cover on splice performance. In the lattice model, the reinforcement-concrete interface properties are treated as inherent parameters and remain constant across specimens with different confinement levels. The simulations enable a detailed examination of how confinement modifies internal crack propagation and stress redistribution. Furthermore, the use of Delaunay triangulation-based meshing is shown to be critical in realistically reproducing strut-cracking behavior and conical stress transfer, thereby capturing confinement effects without modification of interface parameters.

From an engineering perspective, the discrete lattice model also provides added value beyond conventional phenomenological test observations. By explicitly representing fracture processes in the concrete surrounding lap splices, the model affords deeper insight into the internal cracking mechanisms governing reinforcement-concrete bond failure, complementing and enriching the macroscopic descriptions obtained from experimental studies. Taken together with the previous development of a calibration-free approach for determining interface properties [36], the present study establishes a consistent methodological framework that enables the discrete lattice model to be reliably extended from *meso*-scale fracture simulations of cementitious materials to structural-scale analyses of reinforced concrete members under varying confinement conditions.

2. Overview of discrete lattice model

2.1. Modelling procedure of reinforced concrete

The lattice model, originally developed for analyzing the fracture of brittle solids [30], is utilized in this study to simulate the bond behavior of lap-spliced reinforcement in concrete. In this model, the concrete, reinforcement, and reinforcement-concrete interface are discretized into beam elements, each assigned linear elastic properties (including elastic modulus, Poisson's ratio, tensile and compressive strength). External loads are applied in steps to the discrete system under specific boundary conditions. During each loading step, a linear elastic analysis is performed, and the element with the highest stress-to-strength ratio is removed. Note that although beam elements are employed to represent all phases in the model, only the axial (normal) stress and strength will be

considered when calculating the element's stress-to-strength ratio. After that, the stresses of all elements are released before proceeding to the next loading step. This process is repeated sequentially until the target load or displacement is achieved.

The modeling procedures can be described as follows (see simplified 2D representation in Fig. 1):

(1) Creation of the lattice mesh and concrete nodes: a square mesh (cubic for a 3D model) with a size of L_v is generated. Within each voxel, a concrete node is randomly located within a sub-voxel of size L_s. The ratio of the two voxel sizes, L_s/L_v, represents the randomness of concrete nodes and is typically set to 0.5 to reflect the heterogeneity of concrete materials [31,35,36,38,39].

(2) Generation of concrete elements (orange in Fig. 1): the closest pairs of concrete nodes are connected by concrete beam elements according to Delaunay triangulation rules [40]. Although the concrete elements are assigned linear elastic properties, the model can effectively simulate the quasi-brittle behavior of concrete with softening due to the geometric randomness of the lattice mesh [38,41].

(3) Generation of reinforcement nodes and elements (red in Fig. 1): reinforcement is implemented by defining its geometry. Then additional reinforcement nodes are defined at the intersections of the reinforcement and the square (cubic) mesh, and these nodes are connected by reinforcement elements. To represent the plasticity of steel reinforcement during the yielding stage, a multi-segmental fracture law is employed. That is, elements are not removed immediately upon reaching their initial segmental strength but are instead updated with subsequent segmental properties.

(4) Generation of interface elements: reinforcement nodes are connected to their corresponding concrete nodes by interface elements within the same voxel. These elements are also assigned multi-segmental properties to simulate the bond-slip behavior of reinforcement in concrete.

(5) Defining boundary conditions and applying load: boundary conditions are defined, and then loads are applied using a load- or displacement-control scheme.

2.2. *Reinforcement-concrete bond properties*

The reinforcement-concrete bond behavior plays a dominant role in the structural performance of reinforced concrete. Over the decades, various analytical models have been developed to describe the bond stress-slip relationship of steel reinforcement embedded in concrete, with the model proposed by Harajli et al. [12,24] being one of the most comprehensive. This model accounts for the effects of concrete strength, reinforcement rib spacing, and confinement conditions. As shown in Fig. 2, under poor confinement, splitting failure of the concrete can occur, leading to a sudden decrease in bond stress. As confinement is increased, bond strength improves until pull-out failure occurs. This suggests that the bond stress-slip curve under pull-out failure serves as an envelope for all possible curves, beyond which further confinement does not enhance bond strength. In order words it seems that this is intrinsic reinforcement-concrete bond property which is not influenced by the specimen geometry, confinement and boundary conditions.

In the discrete lattice model, the bond between reinforcement and concrete is treated as an inherent property and is independent of varying reinforcement confinement conditions (e.g., concrete cover thickness, stirrup ratios). Therefore, the bond stress-slip relationship under pull-out failure (i.e., the envelope in Fig. 2) should be applied as input. Gu et al. [36] established a mathematical method, based on stochastic analysis considering lattice mesh randomness, to transform the preferred bond stress-slip relationship into the input properties of reinforcement-concrete interface beam elements. Using Delaunay triangulation for meshing, the fundamental conical stress transfer mechanism along reinforcement is captured in the lattice model, even though the steel ribs are not explicitly modelled. The effect of boundary conditions, such as concrete cover thickness, on reinforcement bond behavior is naturally reflected without altering the inputted properties of interface and material elements. This simplified reinforcement-concrete interface modeling approach, with a strong physical foundation, bridges a crucial gap, allowing the lattice model to be scaled from micro/*meso*-scale material simulations to macro-scale structural simulations.

In this research, the reinforcement-concrete interface lattice modeling approach from [36] is adopted to simulate, analyze and understand better the bond failure mechanism of lap-spliced reinforcement in concrete.

3. Validation of discrete lattice model in simulating bond behavior of lap-spliced reinforcement in concrete

The four-point bending test more accurately reflects the stress state of concrete in real structures compared to pull-out bond tests [12,14,42]. Although pull-out tests are convenient, they generate highly localized compressive stress concentrations in concrete around the bar exit point, which do not realistically represent the stress conditions in reinforced concrete members. In contrast, beam-

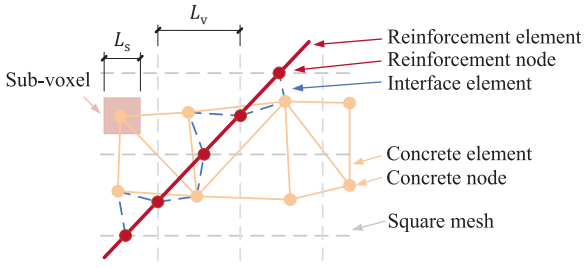

Fig. 1. 2D representation of the lattice mesh for reinforced concrete.

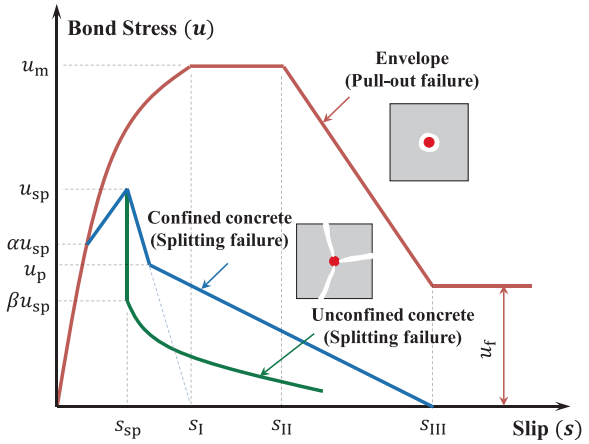

Fig. 2. The analytical bond stress-slip relationship of steel reinforcement embedded in concrete proposed by Harajli et al. [12,24].

type tests such as the four-point bending test are able to reproduce more realistic stress distributions and crack patterns, thus providing more representative insights into reinforcement-concrete bond behavior. Therefore, the beam testing scheme is adopted to investigate the confinement effect on reinforcement-concrete bond behavior using the discrete lattice model.

3.1. Specimen details and testing scheme

To validate the discrete lattice approach for modeling the bond behavior of lap-spliced reinforcement in concrete, the experimental work conducted by Harajli et al. [12] served as a reference. Fig. 3 illustrates the specimen dimensions and splice details. In that study, a simply supported beam specimen was loaded with two symmetrical point loads to produce a constant moment region. The beams were tested under displacement control with a loading rate of approximately 2 mm/min to simulate static loading conditions. The testing parameters include the reinforcement diameter (d_b), the ratio of cover thickness to reinforcement diameter (c/d_b), and the confinement provided by stirrups. The side cover thickness and bottom cover thickness are equal to cover thickness (c), and the splice length is established as $5d_b$. To assess the confinement effect on the reinforcement-concrete bond, two stirrups are positioned in the lap-spliced region, each located at $l_s/4$ from the mid-span. Two linear variable differential transformers are installed at the beam ends to measure reinforcement slip, while strain gauges are attached to the lap-spliced reinforcement at $l_s/2$ from the mid-span. Using the measured reinforcement strain, the reinforcement stress (f_s) can be calculated based on the tested stress–strain relationship of steel. Consequently, the average bond stress (u) within l_s can be determined as follows:

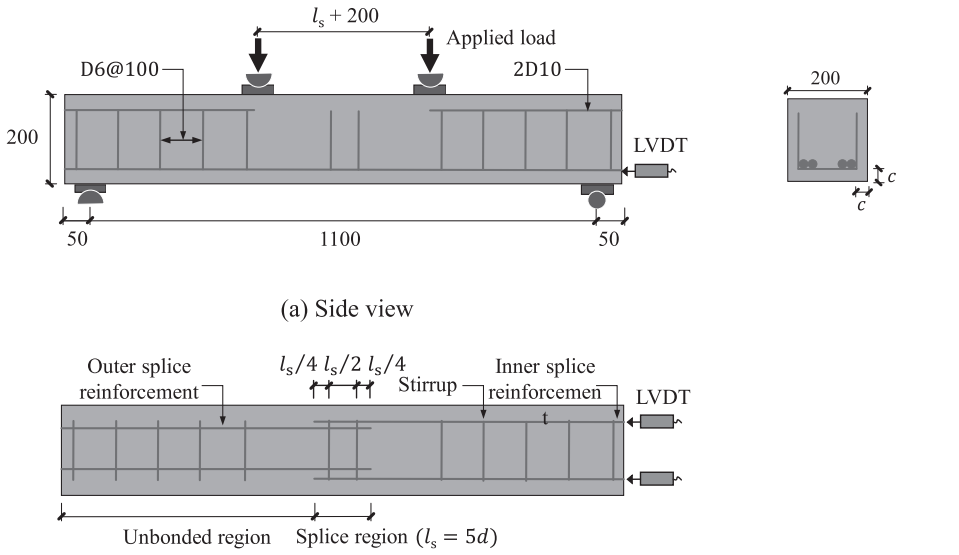

Fig. 3. Specimen dimensions and reinforcement details.

$$u = \frac{A_r f_s}{\pi d_b l_s} \tag{1}$$

where A_r is the cross-sectional area of reinforcement.

The design parameters for all specimens are presented in Table 1. The diameters of the lap-spliced reinforcement are 16, 20, 25, and 32 mm. Varying confinement conditions are achieved by utilizing stirrups of different diameters. Regarding the specimen nomenclature, 'S0′ represents plain cases with no stirrup confinement in the mid-span, while 'S6′ and 'S10′ represents the stirrup confinement cases. The concrete compressive strength f_c' ranged from 39.0 MPa to 43.2 MPa, and the yield strength of the reinforcement was 413.8 MPa. A four-point bending load is applied to the top of all beam specimens, with the lap splices located within the pure bending region.

3.2. Numerical model

To discretely simulate the internal cracking and bond behavior between the lap-spliced reinforcement, it is mandatory to maintain a throughout provision of the interface element between the lap-spliced reinforcement, which requires a minimum benchmark of one Voronoi element. Considering the set benchmark, a mesh size of 8 mm is adopted to generate the lattice model following the procedures outlined in Section 2.1. The effect of mesh size on the bond behavior simulation has been previously confirmed.

In the discrete lattice model, concrete elements are assumed to be linearly elastic and defined by five parameters: element radius (R), elastic modulus (E), shear modulus (G), tensile strength (f_t), and compressive strength (f_c). The elastic modulus and shear modulus are directly assigned as those of the bulk concrete, while R, f_t, and f_c are calibrated through numerical simulations of uniaxial tension and compression tests on concrete cylinders (150 mm × 150 mm × 300 mm), as shown in Fig. 4 (note that the sharp decrease and increase of load derives from the element removal/update procedure used in the beam lattice approach). In this procedure, R is adjusted to match the target elastic modulus, f_t to match the tensile strength, and f_c to match the compressive strength of concrete at macroscopic level. Since the reference experiments did not provide concrete tensile strength or elastic modulus, these values were derived according to Model Code 2010 [43] based on the measured compressive strength. The calibrated parameters used in this study are summarized in Table 2. Although the concrete element is assigned linear elastic constitutive relationships, the post-peak behavior of material can be well captured due to the geometric heterogeneity of lattice mesh.

Unlike the concrete elements, the properties of the reinforcement elements and the reinforcement-concrete interface elements are determined without calibration. The uniaxial stress–strain curve of the steel reinforcement is divided into 10 segments (Fig. 5(a)), each representing linear elastic constitutive relationships, which are then assigned to the reinforcement elements. As clarified in Section 2.2, the steel reinforcement-concrete bond stress-slip model proposed by Harajli et al. [12] for pull-out failure modes (as shown by the envelope curve in Fig. 2) is employed to determine the elemental properties of the reinforcement-concrete interface. In this model, the bond stress-slip relationship corresponding to pull-out failure is defined as an inherent property of the reinforcement-concrete interface elements, governed primarily by concrete strength and reinforcement diameter and rib spacing, and independent of external confinement conditions such as cover thickness or stirrup ratio. These interface properties are kept constant across all simulations. The influence of varying confinement is instead captured naturally through the fracture response of the surrounding concrete in the lattice mesh. Accordingly, if the bond is sufficiently strong to induce splitting failure under low confinement, this outcome emerges directly from the model rather than from any modification of the interface parameters. Therefore, only parameters s_I, s_{II}, s_{III}, u_m, and u_f from Harajli's model are relevant, where $s_I = 0.15c_0$, $s_{II} = 0.35c_0$, $s_{III} = c_0$, $u_m = 2.57\sqrt{f_c'}$, $u_f = 0.35u_m$ (c_0 is clear distance between the ribs on bars, f_c' is cylindrical concrete compression strength, and u_m and u_f are peak and residual bond strength). The bond stress-slip envelope curve is divided into 15 segments, each representing a linear elastic constitutive relationship, as illustrated in Fig. 5 (b).

The mechanical properties of the reinforcement-concrete interface elements are, however, inherently linked to the discretization, since the definition of "per unit bar length" is mesh dependent and corresponds to the interface element length. When a coarser mesh is used, each interface element represents a longer bar segment and its transfer capacity must be scaled accordingly. The determination procedure is as follows: (1) the elastic modulus of the interface element is initially assumed equal to that of concrete; (2) the element radius is then calibrated so that the bond stiffness per unit bar length matches the target value; and (3) with the element radius fixed, the tensile and compressive strengths are scaled to ensure that the bond strength per unit bar length also equals the target value. To avoid a trial-and-error calibration, a quantitative method was established in authors' previous study [36], enabling direct calculation

Table 1
Parametric details of the test specimens used for numerical evaluation.

Specimens	Concrete compressive strength f_c' (MPa)	Splice diameter d_b(mm)	Cover thickness c(mm)	c/d_b	Splice length l_s(mm)	Stirrup diameter d_s(mm)	Space s(mm)
B1W-S0	40.7	16	34	2.1	80	/	/
B1W-S6	40.7					6	40
B1W-S10	43.2					10	40
B2W-S0	39.0	20	30	1.5	100	/	/
B3W-S0	40.7	25	25	1.0	125		
B4W-S0	39.0	32	18	0.56	160		

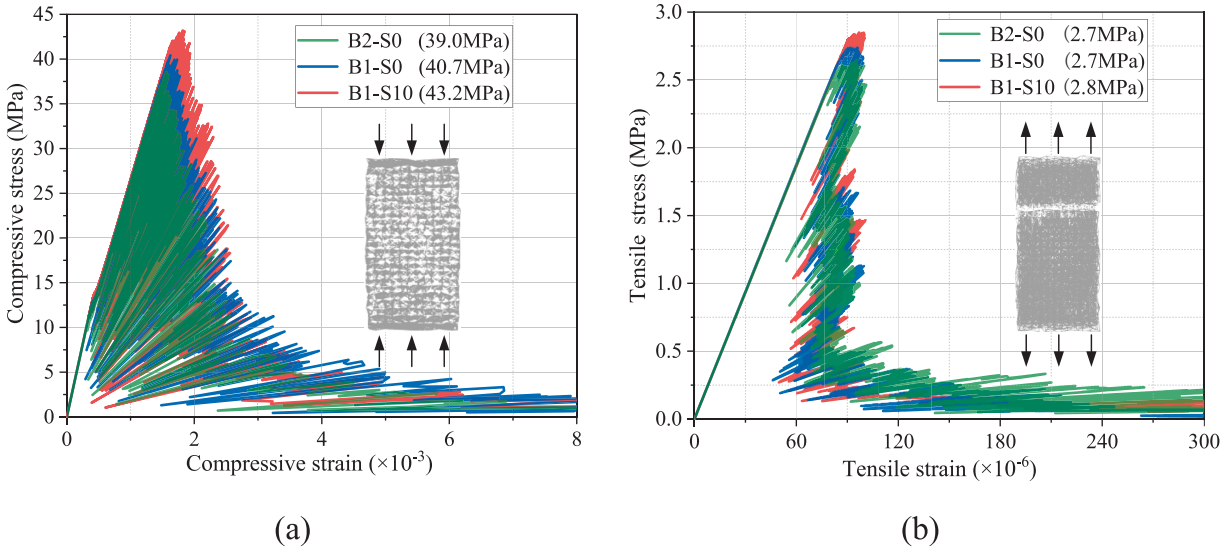

Fig. 4. Calibrated stress–strain behavior of concrete under (a) uniaxial compression and (b) tension.

Table 2
Calibrated concrete element properties in the lattice model for each lap-spliced specimen.

Specimens	*R*(mm)	*E*(MPa)	*G*(MPa)	f_t(MPa)	f_c(MPa)
B1W-S0	3.36	31,140	12,976	3.6	72.0
B1W-S6				3.6	72.0
B1W-S10				3.8	78.0
B2W-S0	3.36	31,140	12,976	3.5	68.0
B3W-S0				3.6	72.0
B4W-S0				3.5	68.0

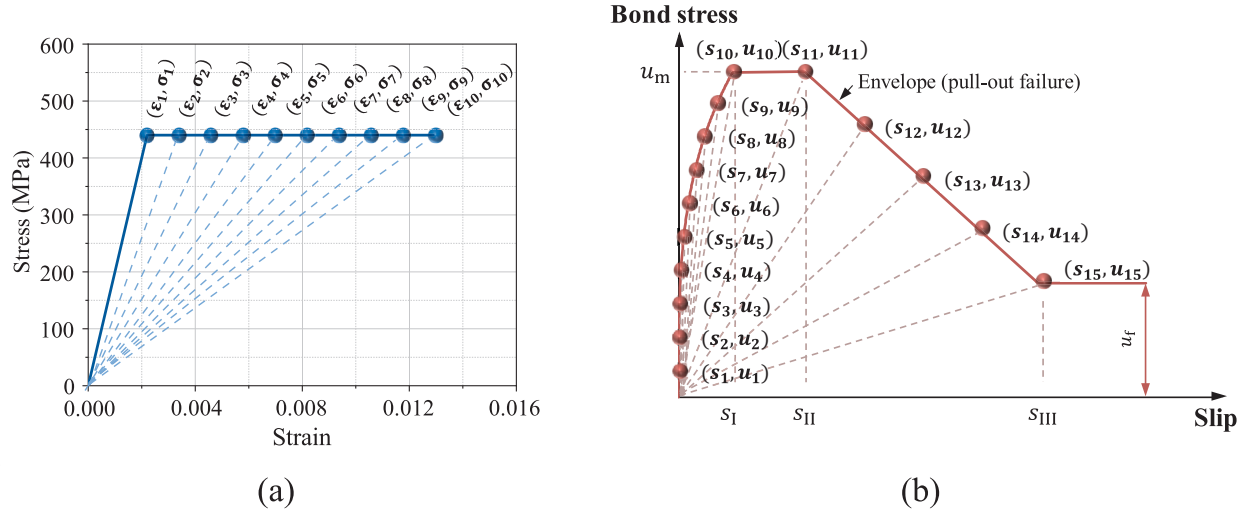

Fig. 5. Input of element properties (a) reinforcement elements (b) bond stress-slip relationship (monotonic envelope model of pull-out failure suggested by Harajli [12,24]).

of the interface element properties from fundamental parameters such as concrete strength, reinforcement diameter, rib spacing, and mesh size. The derived formulations, based on stochastic analysis, are expressed in Eqs. (2)-(5):

$$\sqrt{\frac{u_1 D}{E_c s_1}} \cdot \frac{L_v}{2} \tag{2}$$

$$= \frac{u_n D L_v^2}{4 s_n r^2 \mathrm{E}\left[\frac{K_{n,\text{non-aligned}}}{K_{n,\text{aligned}}}\right]} \tag{3}$$

$$G_n = \frac{E_n}{2(1+\nu)} \tag{4}$$

$$f_n = \frac{D L_v u_n}{2 r^2 \mathrm{E}\left[\frac{u_{n,\text{non-aligned}}}{u_{n,\text{aligned}}}\right]} \tag{5}$$

where D is the diameter of the reinforcement, and r is the radius of the interface element. Note that L_v is assigned the mesh size value. For the nth segment of input, E_n is the elastic modulus, G_n the shear modulus, ν the Poisson's ratio of the interface element, and f_n the interface element strength for nth segment. The coefficients $\mathrm{E}\left[\frac{K_{n,\text{non-aligned}}}{K_{n,\text{aligned}}}\right]$ and $\mathrm{E}\left[\frac{u_{n,\text{non-aligned}}}{u_{n,\text{aligned}}}\right]$ represent the expectation of the bond strength ratio and bond stiffness ratio between reinforcement with aligned and non-aligned interface elements, which are dependent on mesh randomness and relative location of reinforcement embedded in the mesh [36]. The interface element parameters derived of two representative reinforcement types are shown in Table 3.

3.3. Bond stress-slip behavior and failure mode

The experimental and numerical bond stress-slip relationships within the lap-spliced regions of beams with different c/d_b ratios and stirrup confinement are illustrated in Fig. 6(a) and Fig. 6(b), respectively. To eliminate the effect of varied concrete strength in different specimens, the measured bond stress is normalized by $1/\sqrt{f_c'}$.

As illustrated in Fig. 7(a) and Fig. 7(b), the numerical results exhibit reasonable consistency with experimental data across various c/d_b ratios and stirrup confinement, with the ratio of predicted bond strength ($u_{max,pre}$) to the tested bond strength ($u_{max,exp}$) ranging from 1 %~7 %. Without altering the properties of the reinforcement-concrete interface elements, the lattice model well simulates the decrease in bond strength (u_{max}) as the c/d_b ratio or stirrup confinement is reduced. Additionally, the simulations accurately replicate the pre-peak stiffness degradation with increasing slip, accompanied by the progression of bending cracks and the subsequent extension of splitting cracks towards the beam surface. Furthermore, the sudden drop in bond stress observed during the post-peak stage in beams without stirrups, indicating brittle bond failure of the lap splices, is also accurately captured. The crack patterns of above simulated beams are shown in Fig. 8. Clearly, splitting failure within the lap-spliced region occurs in all beam specimens, consistent with the experimental observations. In beams without stirrup confinement, lap splices exhibit noticeable lateral dilatancy, while in beams with stirrups, the crack width and lateral dilatancy are effectively restricted. The reference experiment by Harajli et al. [12] only reported bond stress-slip responses, without providing crack patterns or failure photographs. Therefore, a direct visual comparison was not possible. Nevertheless, the simulations reproduced the experimental bond stress-slip curves and revealed a bond splitting failure mode, consistent with the qualitative description in [12]. Moreover, the simulated crack patterns exhibit a high degree of similarity to those reported in related experimental investigations, such as [44] and [11].

Table 3
Reinforcement-concrete interface parameters used as input in the lattice simulation of representative specimen B1W-S10 (stirrup diameter is 8 mm, longitudinal reinforcement diameter is 16 mm).

$n$thsegment	Stirrup-concrete interface elements r = 6.02 mm			Longitudinal reinforcement-concrete interface elements r = 5.46 mm				
	E_n(MPa)	G_n(MPa)	f_{tn}(MPa)	f_{cn}(MPa)	E_n(MPa)	G_n(MPa)	f_{tn}(MPa)	f_{cn}(MPa)
1	48,732	20,305	1.44	−1.44	112,010	46,673	5.98	−5.98
2	9670	4029	2.88	−2.88	22,226	9261	11.96	−11.96
3	3754	1564	4.31	−4.31	8629	3596	17.94	−17.94
4	1919	799	5.75	−5.75	4410	1837	23.93	−23.93
5	1140	475	7.19	−7.19	2620	1091	29.91	−29.91
6	745	310	8.63	−8.63	1712	713	35.89	−35.89
7	520	217	10.06	−10.06	1195	498	41.87	−41.87
8	381	159	11.50	−11.50	875	365	47.85	−47.85
9	289	121	12.94	−12.94	665	277	53.83	−53.83
10	226	94	14.38	−14.38	520	217	59.82	−59.82
11	97	40	14.38	−14.38	223	93	59.82	−59.82
12	55	23	12.04	−12.04	127	53	50.10	−50.10
13	34	14	9.70	−9.70	78	32	40.38	−40.38
14	21	9	7.37	−7.37	48	20	30.66	−30.66
15	12	5	5.03	−5.03	27	11	20.94	−20.94

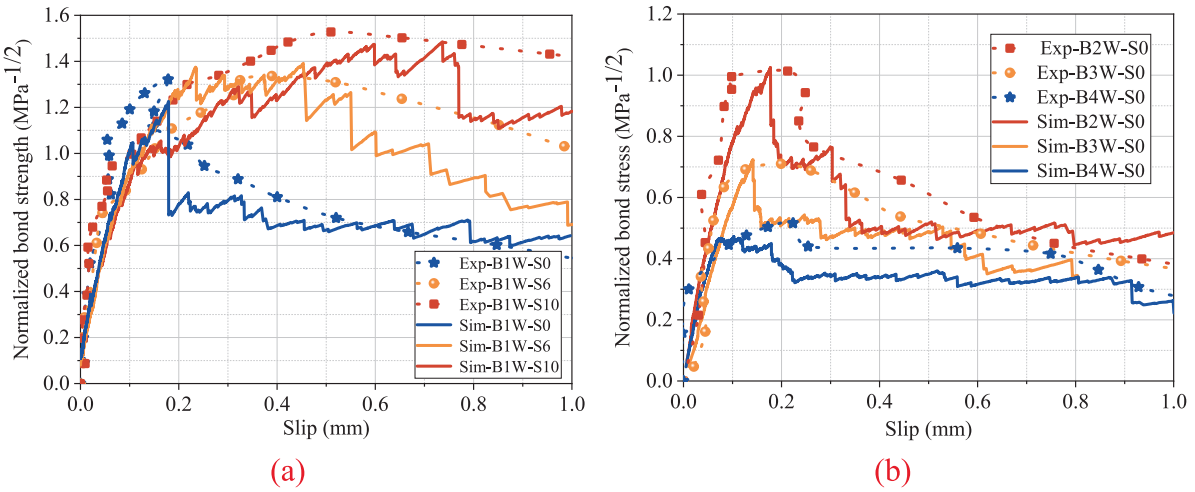

Fig. 6. Experimental and simulated bond stress-slip behavior in beams with different (a) c/d_b ratios (B2W-S0, B3W-S0, B4W-S0); (b) stirrup confinement (B1W-S0, B1W-S6, B1W-S10).

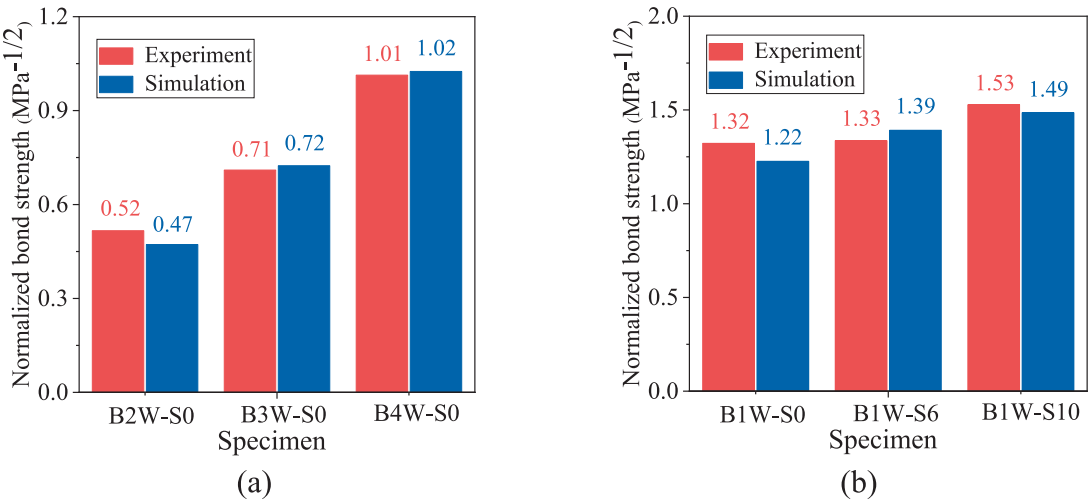

Fig. 7. Normalized bond strength in beams with different (a) c/d_b ratios (B2W-S0, B3W-S0, B4W-S0); (b) stirrup confinement (B1W-S0, B1W-S6, B1W-S10).

4. Bond failure mechanism of unconfined lap-spliced reinforcement

To better understand the bond failure mechanism of unconfined lap-spliced reinforcement, this section further analyzes the crack propagation, internal fracture processes, and compressive strut action in the representative specimen B1W-S0.

4.1. Crack propagation

The crack patterns of specimen B1W-S0 corresponding to different slip levels are shown in Fig. 9. Under four-point bending, the initial flexural crack occurs on the bottom of the beam outside the lap-spliced region. As the peak load is reached, a flexural crack also appears within the lap-spliced region. Subsequently, several splitting cracks develop on the bottom of the beam, corresponding to the bond degradation of the lap splices. At a slip of 0.74 mm, the concrete in the lap-spliced region has severely split into multiple fragments, providing limited confinement to facilitate effective bond stress transfer.

4.2. Internal fracture process

In addition to the crack propagation as observed on surface, the lattice model can provide valuable insights into the internal fracture process of the simulated specimen, as shown in Fig. 10 and Fig. 11. Until reaching the slip value of approximately 0.03 mm

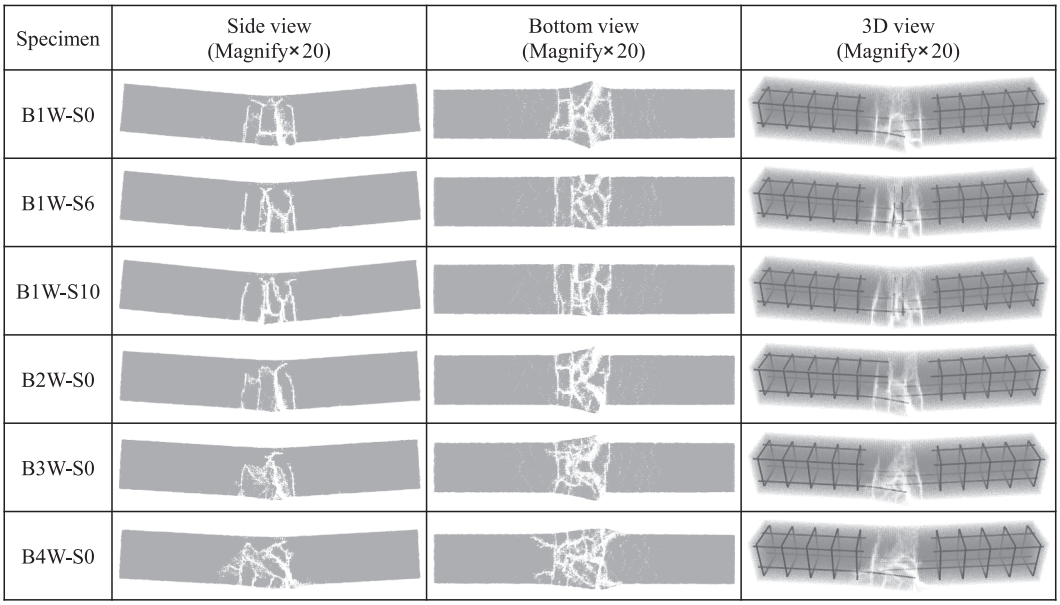

Fig. 8. Crack patterns of simulated beams at ultimate failure.

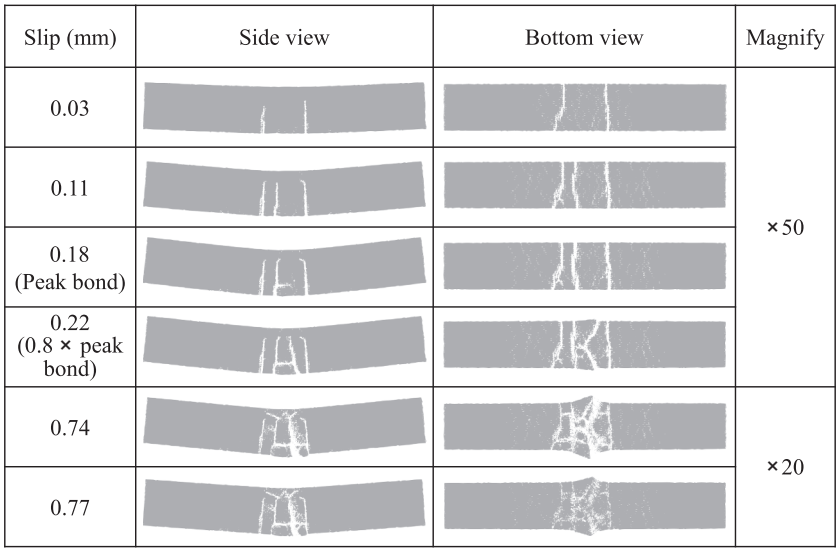

Fig. 9. Simulated crack propagation in the beam specimen B1W-S0.

(corresponding to the moment A in Fig. 11), two flexural cracks successively develop outside the lap-spliced region, with no cracks observed between the lap-spliced reinforcements. The fractured ligaments exhibit two subsequent peaks, corresponding to the formation of two flexural cracks. When the slip reaches approximately 0.11 mm (corresponding to the moment B in Fig. 11), another flexural crack forms inside the lap-spliced region. The fractured ligaments exhibit another peak corresponding to a subsequent decrease in bond stiffness. When the slip reaches approximately 0.18 mm (corresponding to the moment C in Fig. 11), the peak bond strength is reached. Subsequently, with increased slip the bond stress significantly decreases, along with strut cracks occurring between the lap-spliced reinforcement. When the slip reaches approximately 0.22 mm (corresponding to the moment D in Fig. 11), the strut cracks interlink and extend, indicating reduced confinement capacity of concrete cover within the lap-spliced region and subsequent decrease in normalized bond stress. As the slip increases without the formation of new peaks in the fractured ligaments, splitting failure eventually develops within the lap-spliced region.

In summary, the fracture process of lap splices is characterized by flexural cracks at the beam's bottom initially, followed by the formation of strut cracks between the lap-spliced reinforcement. As strut cracks interlink and extend, dilatancy and splitting of the concrete cover within lap-spliced region occurs, lead to the splitting failure of unconfined lap splice.

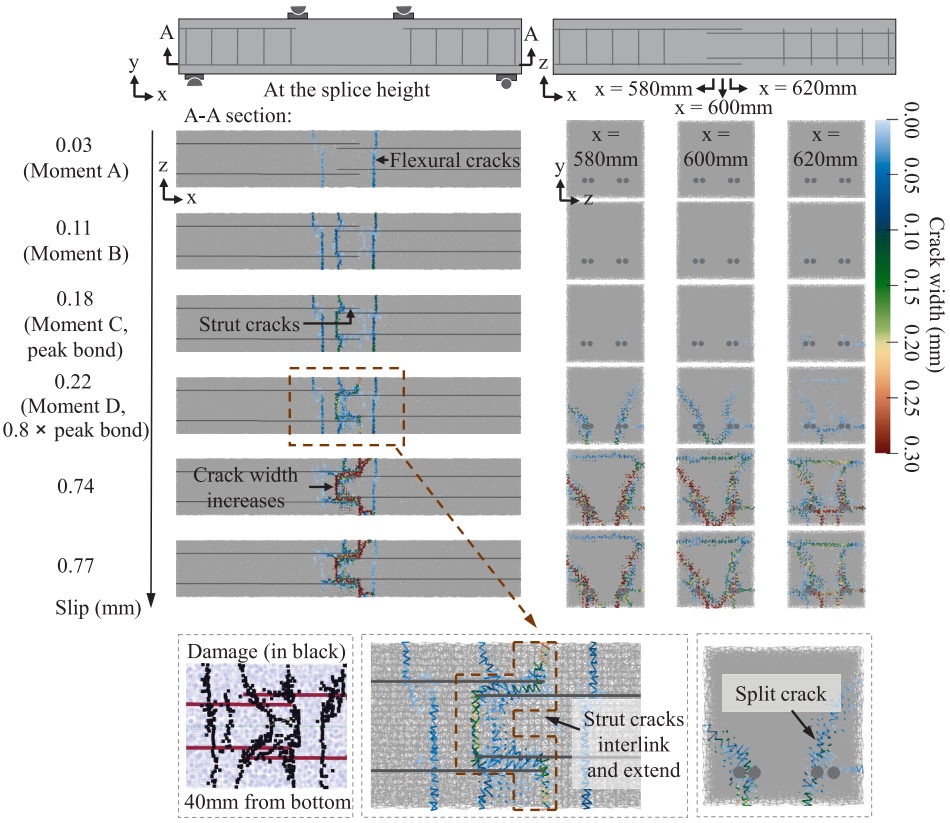

Fig. 10. Internal crack in the beam specimen B1W-S0.

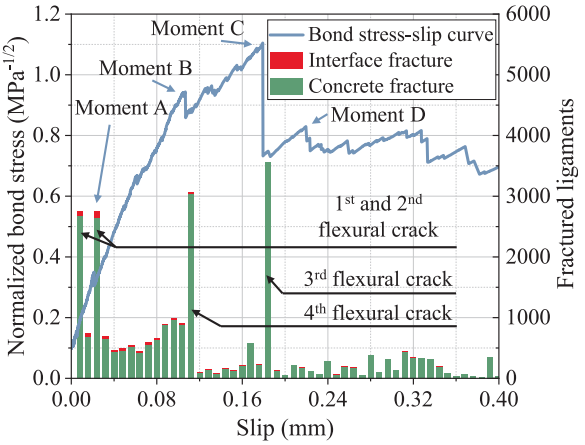

Fig. 11. Fractured ligaments in the beam specimen B1W-S0.

4.3. Compressive struts between splices

To further illustrate the bond failure mechanism of unconfined lap splices, the internal stress distribution of the simulated specimen is shown in Fig. 12. The so-called conical stress transfer mechanism, often described in design codes and experimental studies of bond behavior, refers to the transfer of bond force from the reinforcement to the surrounding concrete through inclined compressive struts that spread out in a conical manner from the bar ribs [12,42,43]. This phenomenon is clearly reproduced in the present simulations, as highlighted by the schematic illustration in Fig. 13 included for clarity.

When the slip reaches approximately 0.03 mm, compressive struts form between lap-spliced reinforcements. As the slip increases, the conical stress transferring area expands. When the slip reaches approximately 0.18 mm, peak bond strength is reached. At this

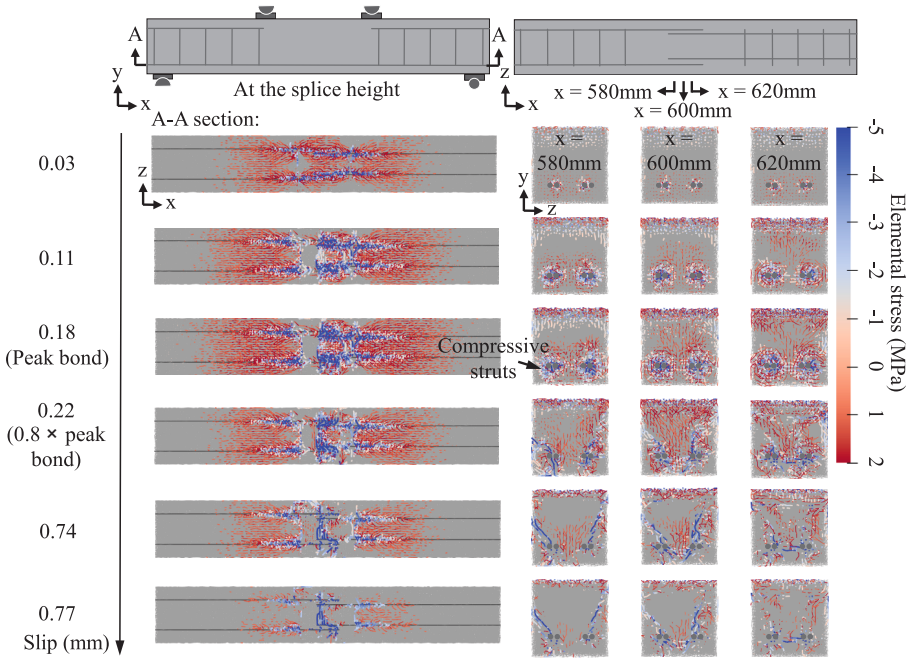

Fig. 12. Concrete stress distribution in the beam specimen B1W-S0.

point, concrete elements at the boundary are subjected to compression. When the slip reaches approximately 0.22 mm, the circular compressive field at the splice height on the cross section transforms into inclined compressive flows. During the post-peak stage, the conical stress transferring area reduces due to the splitting and the reduced confinement capacity of concrete cover within lap-spliced region.

5. Confinement effect of stirrups in enhancing the bond of lap splices

Stirrup confinement enhances the peak bond strength of lap splices, as shown in section 3.3. To unveil the effect of stirrup confinement on the reinforcement-concrete bond behavior, this section further analyzes the crack propagation, internal fracture process, and stress distribution along stirrups in the representative specimen B1W-S10.

5.1. Crack propagation

The crack patterns of specimen B1W-S10 corresponding to the same slip levels with specimen B1W-S0 are shown in Fig. 14. During the initial stage, flexural cracks occur on the bottom of the beam, with several splitting cracks developing from the bottom of the beam. As the peak load is reached, the concrete in the lap-spliced region has been split into multiple fragments, while the lateral dilatancy is effectively restricted by the stirrup confinement.

5.2. Internal fracture process

The internal crack development in the beam specimen B1W-S10 is shown in Fig. 15. During the initial loading stage, internal crack development in the beam specimen B1W-S10 is similar to that in the beam specimen B1W-S0. When the slip reaches approximately 0.03 mm, one flexural crack first develops outside the lap-spliced region, resulting in a peak in fractured ligaments (corresponding to the moment A in Fig. 16). When the slip reaches approximately 0.11 mm, another flexural crack forms outside the lap-spliced region with a new peak in fractured ligaments (corresponding to the stage between moment A and moment B in Fig. 16). When the slip reaches approximately 0.18 mm, strut cracks occur between the lap-spliced reinforcement. The peak bond stress is reached at a slip of 0.74 mm when the cross-section is split into several pieces by internal cracks. As the stirrup legs can bridge the cracks, a ductile bond failure mode is achieved.

5.3. Stress distribution along stirrups

The stress distribution inside the beam is illustrated in Fig. 17. During the initial loading stage, compressive struts form and extend between lap-spliced reinforcements. When the slip reaches approximately 0.74 mm, peak bond strength is reached. The high tensile stress (reaching a maximum of 106.1 MPa) in the stirrups, along with the large compressive stress field within them, demonstrates that

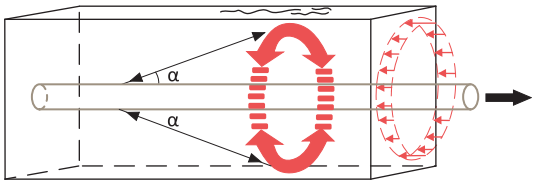

Fig. 13. Schematic representation of how the radial components of the bond forces are balanced against tensile stress rings in the concrete in a conical manner [42].

Slip (mm)	Side view	Bottom view	Magnify
0.03			×50
0.11			
0.18			
0.22			
0.74 (Peak bond)			×20
0.77 (0.8 × peak bond)			

Fig. 14. Simulated crack propagation in the beam specimen B1W-S10.

the stirrups effectively restrict dilatancy and splitting of the concrete within the lap-spliced region, acting as passive confinement. Throughout the entire loading stage, the conical stress transfer area remains intact as the slip increases, enabling the concrete within the lap-spliced region to transfer higher bond stress compared to the reference beam without stirrup confinement.

6. Dominant role of Delaunay triangulation-based mesh in simulating realistic bond stress transfer

From the previous analysis of fracture processes and stress distribution, it is evident that accurately simulating the formation of strut cracks and the dilatancy of the concrete within the lap-spliced region is crucial for reflecting the effect of confinement on bond behavior. The Delaunay triangulation-based mesh is considered essential for facilitating the development of compressive strut stress. To demonstrate the role of the Delaunay triangulation-based mesh, representative beam specimens (B1W-S0, B1W-S10) with a regular quadrangle mesh are modeled using the lattice model.

The simulated bond stress-slip curves for lap splices, using both Delaunay triangulation-based and regular quadrangle meshes, are shown in Fig. 18(a) and Fig. 18(b), respectively. The bond strength of lap splices simulated with the regular quadrangle mesh is significantly lower than the one with Delaunay triangulation-based mesh and experimental results.

The simulated crack patterns using a regular quadrangle mesh are shown in Fig. 19, while a schematic diagram illustrating the bond stress transfer in both regular quadrangle and Delaunay triangulation-based meshes is provided in Fig. 20 and Fig. 21. In the experiments, the radial component of the gripping force on the reinforcement ribs induces cracks in the surrounding concrete at angles ranging from 45° to 60° [45]. However, when concrete is modeled using a regular quadrangle mesh, stress can only be transferred along grid boundaries at 90°, limiting the ability to simulate strut cracks and the conical stress distribution. Consequently, the beam specimen with the regular quadrangle mesh fails to capture the dilatancy of the concrete, thereby preventing the stirrups from providing effective passive confinement.

In contrast, in the beam specimen with a Delaunay triangulation-based mesh, shear stress on the reinforcement surface is transferred along inclined angles, accurately simulating the strut cracking behavior and conical stress distribution. Therefore, the lattice model, by using the Delaunay triangulation-based mesh, can naturally reflect the changes in bond stress-slip behavior of specimens under different confinement conditions without needing to modify the properties of the reinforcement-concrete interface elements.

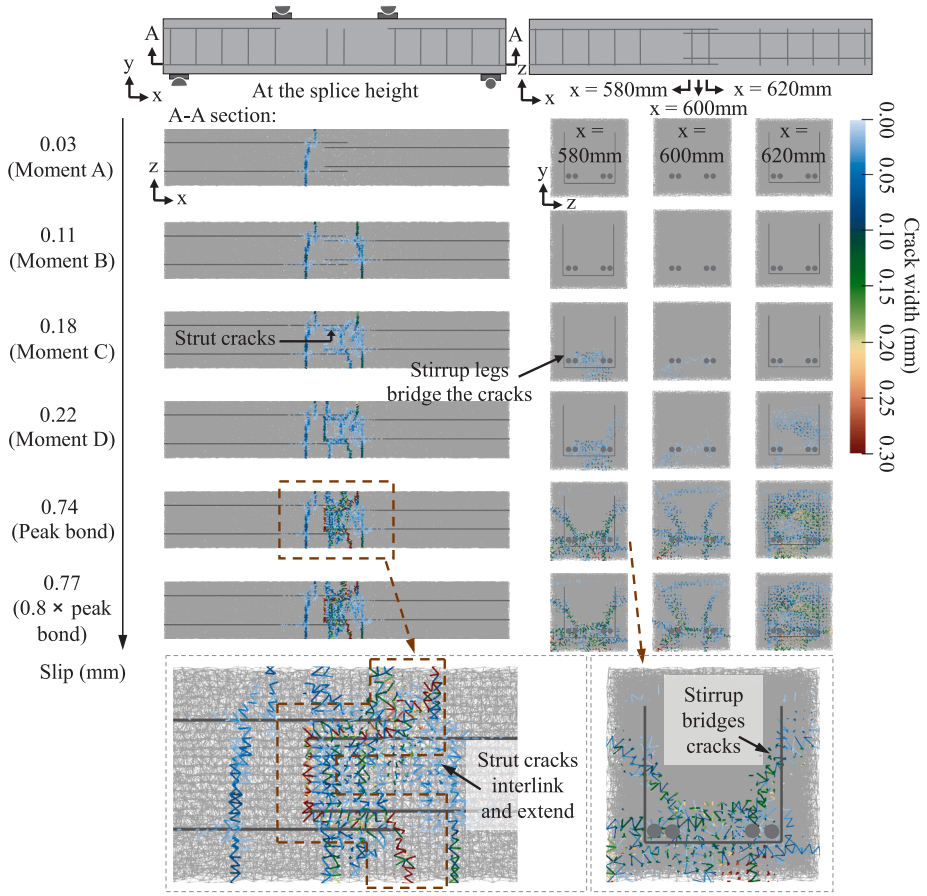

Fig. 15. Internal crack in the beam specimen B1W-S10.

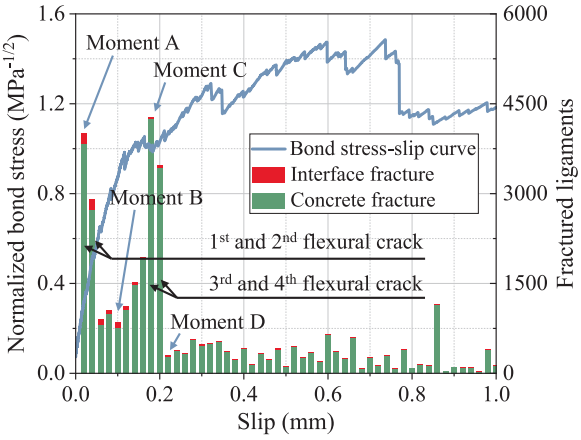

Fig. 16. Fractured ligaments in the beam specimen B1W-S10.

7. Conclusions

In this study, the lattice model is employed to investigate the effect of confinement on the bond behavior of lap-spliced reinforcement. Based on the validated model, a detailed analysis is conducted on how confinement influences reinforcement-concrete bond behavior, including crack propagation, fracture processes, and stress distribution. This study validates the discrete lattice model as a robust framework for macroscopic mechanical analysis of reinforced concrete structures. The model not only reliably predicts bond stress-slip behavior and failure modes under varying confinement conditions, but also provides mechanistic insights into

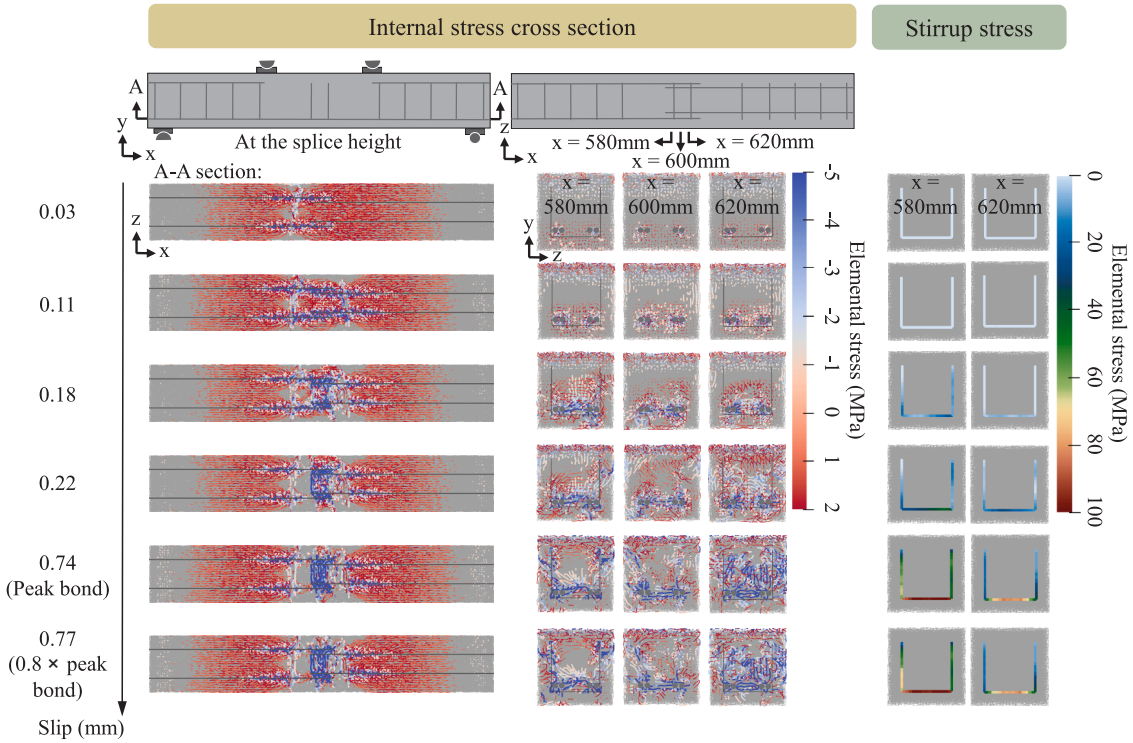

Fig. 17. Concrete and stirrup stress distribution in the beam specimen B1W-S10.

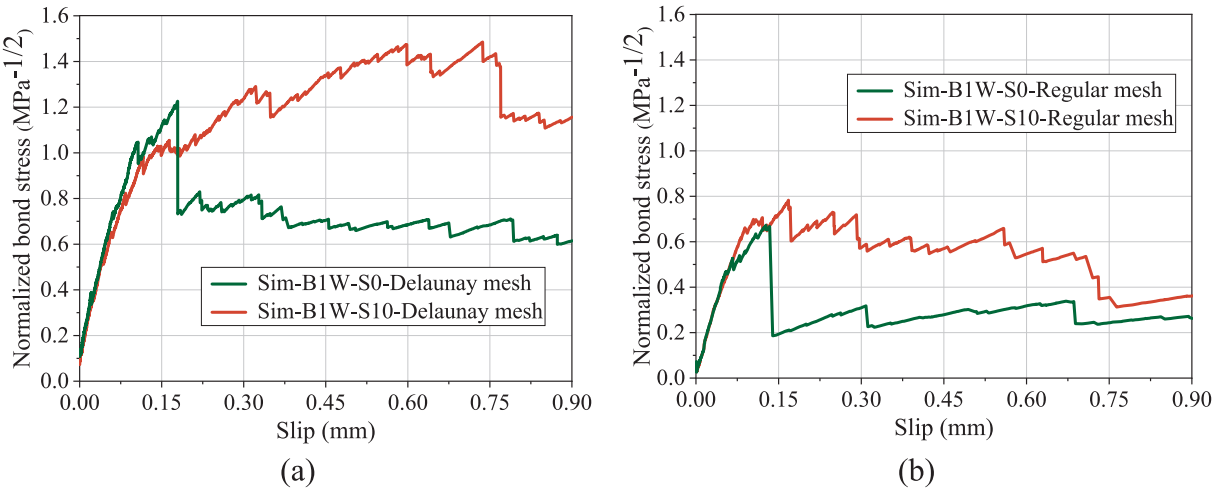

Fig. 18. Simulated bond stress-slip curves in B1W-S10 using (a) Delaunay triangulation-based mesh (b) regular quadrangle mesh.

the internal fracture processes governing bond failure, thereby supporting rational reinforcement detailing in engineering practice. The main conclusions are drawn as follows:

(1) The bond-slip law under pull-out failure is treated as an intrinsic property of the reinforcement-concrete interface in the adopted lattice model. Although the properties of the reinforcement-concrete interface elements and material properties of reinforcement and concrete remain constant in specimens with varying stirrup ratios, the model accurately grasps the influence of confinement provided either by concrete cover or stirrups on reinforcement-concrete bond behavior.

(2) The bond failure of unconfined lap splices is initially characterized by the development of flexural cracks in the beam tensile zone until reaching the peak load, followed by the formation of strut cracks between the lap-spliced reinforcement. As these

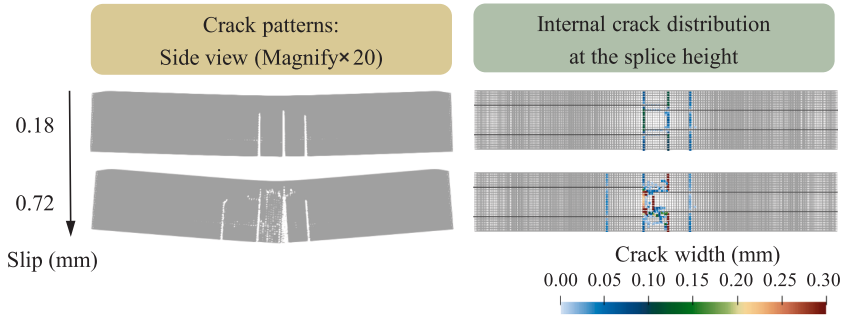

Fig. 19. Simulated crack patterns using regular quadrangle mesh.

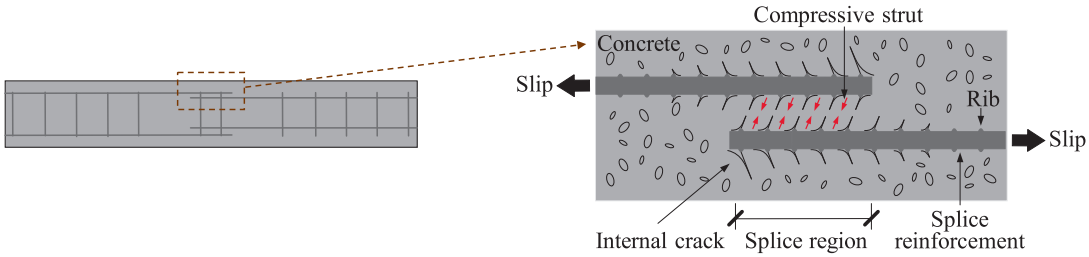

Fig. 20. Schematic diagram illustration of the bond stress transfer.

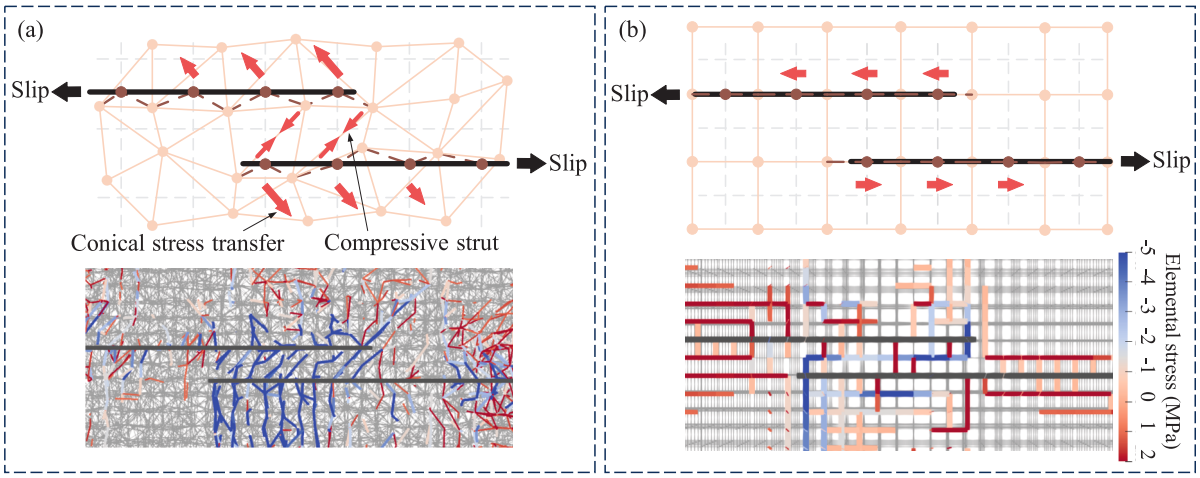

Fig. 21. Schematic diagram illustration of bond stress transfer in (a) Delaunay triangulation-based mesh and (b) regular quadrangle mesh.

strut cracks propagate and interconnect, dilatancy and splitting of the concrete cover within the lap-spliced region occur, ultimately leading to the splitting failure of the unconfined lap splice.

(3) The high tensile stress in the stirrups and the significant compressive stress field in concrete demonstrates that the stirrups can effectively restrict dilatancy and splitting of the concrete within the lap-spliced region, acting as passive confinement. This can be attributed to the preservation of the conical stress transfer area, as the stirrup legs bridge and restrain crack development.

(4) Generating lattice mesh using the Delaunay triangulation scheme can replicate realistic strut cracking behavior and conical stress transfer in lap splices, thereby naturally capturing variations in bond stress-slip behavior under different confinement conditions without requiring modifications to the reinforcement-concrete interface properties.

CRediT authorship contribution statement

Xun Liu: Writing – original draft, Validation, Supervision, Methodology, Investigation, Data curation. **Dawei Gu:** Writing – review & editing, Validation, Methodology, Conceptualization. **Jinlong Pan:** Supervision, Conceptualization. **Mladena Luković:** Writing –

review & editing, Validation, Supervision, Conceptualization.

Declaration of competing interest

The authors declare that they have no known competing financial interests or personal relationships that could have appeared to influence the work reported in this paper.

Acknowledgements

The work is financially supported by the Natural Science Foundation of Jiangsu Province (Project Number: BK20230860), National Natural Science Foundation of China (Project Number: 51778131) and Dutch Organization for Scientific Research (NWO) under the grant “Optimization of interface behavior for innovative hybrid concrete structures” (Project Number: 16814).

Data availability

Data will be made available on request.

References

[1] Yuan H, Bing H. Experimental study on bond behavior between high-strength grout and deformed steel bars. Constr Build Mater 2021;301:124059. https://doi.org/10.1016/j.conbuildmat.2021.124059.
[2] Zhang J, Tao X, Li X, Zhang Y, Liu Y. Analytical and experimental investigation of the bond behavior of confined high-strength recycled aggregate concrete. Constr Build Mater 2022;315:125636. https://doi.org/10.1016/j.conbuildmat.2021.125636.
[3] Shang H, Cui F, Zhang P, Zhao T, Ren G. Bond behavior of steel bar embedded in recycled coarse aggregate concrete under lateral compression load. Constr Build Mater 2017;150:529–37. https://doi.org/10.1016/j.conbuildmat.2017.05.060.
[4] Jiang T, Zhang X, Wu Z, Abdellahi MM. Bond-slip response of plain bars embedded in self-compacting lightweight aggregate concrete under lateral tensions. J Mater Civ Engng 2017;29. https://doi.org/10.1061/(ASCE)MT.1943-5533.0001893.
[5] Long X, Wang C-Y, Zhao P-Z, Kang S-B. Bond strength of steel reinforcement under different loading rates. Constr Build Mater 2020;238:117749. https://doi.org/10.1016/j.conbuildmat.2019.117749.
[6] Ožbolt J, Oršanić F, Balabanić G. Modeling pull-out resistance of corroded reinforcement in concrete: coupled three-dimensional finite element model. Cem Concr Compos 2014. https://doi.org/10.1016/j.cemconcomp.2013.10.014.
[7] Avadh K, Jiradilok P, Bolander JE, Nagai K. Mesoscale simulation of pull-out performance for corroded reinforcement with stirrup confinement in concrete by 3D RBSM. Cem Concr Compos 2021. https://doi.org/10.1016/j.cemconcomp.2020.103895.
[8] Xu L, Wang X, Pan J, Zhou J, Liu W. Bond behavior between steel-FRP composite bars and engineered cementitious composites in pullout conditions. Engng Struct 2024. https://doi.org/10.1016/j.engstruct.2023.117086.
[9] Xu L, Ma X, Pan J, Zhou J, Wang X, Liu W. Investigation on bond behavior of steel-FRP composite bars in engineered cementitious composites by spliced beam tests. Constr Build Mater 2023. https://doi.org/10.1016/j.conbuildmat.2023.133480.
[10] Farooq U, Nakamura H, Miura T. Evaluation of failure mechanism in lap splices and role of stirrup confinement using 3D RBSM. Engng Struct 2022;252:113570. https://doi.org/10.1016/j.engstruct.2021.113570.
[11] Bandelt MJ, Billington SL. Bond behavior of steel reinforcement in high-performance fiber-reinforced cementitious composite flexural members. Mater Struct Constr 2016;49:71–86. https://doi.org/10.1617/s11527-014-0475-4.
[12] Harajli MH, Hamad BS, Rteil AA. Effect of confinement of bond strength between steel bars and concrete. ACI Struct J 2004;101:595–603. https://doi.org/10.14359/13381.
[13] Ronanki VS, Aaleti S, Valentim DB. Experimental investigation of bond behavior of mild steel reinforcement in UHPC. Engng Struct 2018;176:707–18. https://doi.org/10.1016/j.engstruct.2018.09.031.
[14] Committee ACI. 408. Bond and Development of Straight reinforcing Bars in Tension (ACI 408R-03). Farmington Hills, MI: American Concrete Institute; 2003.
[15] Vieito I, Herrador MF, Martínez-Abella F, Varela-Puga F. Proposal and assessment of an efficient test configuration for studying lap splices in reinforced concrete. Engng Struct 2018;165:1–10. https://doi.org/10.1016/j.engstruct.2018.03.004.
[16] Moodi Y, Sohrabi MR, Mousavi SR. Effects of stirrups in spliced region on the bond strength of corroded splices in reinforced concrete (RC) beams. Constr Build Mater 2020;230:116873. https://doi.org/10.1016/j.conbuildmat.2019.116873.
[17] Lemcherreq Y, Zanuy C, Vogel T, Kaufmann W. Experimental and analytical assessment of fatigue damage in reinforced concrete tension members. Engng Struct 2023;289:116306. https://doi.org/10.1016/j.engstruct.2023.116306.
[18] Wu C, Hwang H-J, Ma G. Effect of stirrups on the bond behavior of lap spliced GFRP bars in concrete beams. Engng Struct 2022;266:114552. https://doi.org/10.1016/j.engstruct.2022.114552.
[19] Jakubovskis R, Kaklauskas G. Bond-stress and bar-strain profiles in RC tension members modelled via finite elements. Engng Struct 2019;194:138–46. https://doi.org/10.1016/j.engstruct.2019.05.069.
[20] Ooi ET, Yang ZJ. Modelling crack propagation in reinforced concrete using a hybrid finite element–scaled boundary finite element method. Engng Fract Mech 2011;78:252–73. https://doi.org/10.1016/j.engfracmech.2010.08.002.
[21] Kim T-H, Kim B-S, Chung Y-S, Shin HM. Seismic performance assessment of reinforced concrete bridge piers with lap splices. Engng Struct 2006;28:935–45. https://doi.org/10.1016/j.engstruct.2005.10.020.
[22] Abdelatif AO, Ožbolt J, Gambarelli S. 3D finite element modelling of corrosion of lap splice joints in concrete. Constr Build Mater 2018;169:124–31. https://doi.org/10.1016/j.conbuildmat.2018.02.150.
[23] Seok S, Haikal G, Ramirez JA, Lowes LN. High-resolution finite element modeling for bond in high-strength concrete beam. Engng Struct 2018;173:918–32. https://doi.org/10.1016/j.engstruct.2018.06.068.
[24] Harajli MH. Bond stress–slip model for steel bars in unconfined or steel, FRC, or FRP confined concrete under cyclic loading. J Struct Engng 2009. https://doi.org/10.1061/(asce)0733-9445(2009)135:5(509).
[25] Cusatis G, Pelessone D, Mencarelli A. Lattice discrete particle model (LDPM) for failure behavior of concrete. I: theory. Cem Concr Compos 2011;33:881–90. https://doi.org/10.1016/j.cemconcomp.2011.02.011.
[26] Alnaggar M, Pelessone D, Cusatis G. Lattice discrete particle modeling of reinforced concrete flexural behavior. J Struct Engng 2019;145. https://doi.org/10.1061/(ASCE)ST.1943-541X.0002230.
[27] Bolander JE, Hong GS, Yoshitake K. Structural concrete analysis using rigid-body-spring networks. Comput Civ Infrastruct Eng 2000;15:120–33. https://doi.org/10.1111/0885-9507.00177.
[28] Farooq U, Nakamura H, Miura T, Yamamoto Y. Proposal of bond behavior simulation model by using discretized voronoi mesh for concrete and beam element for reinforcement. Cem Concr Compos 2020;110:103593. https://doi.org/10.1016/j.cemconcomp.2020.103593.

[29] Farooq U, Nakamura H, Miura T. Bond behavior evaluation of deformed rebar dependent on lateral pressure confinement including various structural parameters. Cem Concr Compos 2021;119:103996. https://doi.org/10.1016/j.cemconcomp.2021.103996.
[30] Schlangen E, Garboczi EJ. Fracture simulations of concrete using lattice models: computational aspects. Engng Fract Mech 1997;57:319–32. https://doi.org/10.1016/s0013-7944(97)00010-6.
[31] Luković M, Schlangen E, Ye G. Combined experimental and numerical study of fracture behaviour of cement paste at the microlevel. Cem Concr Res 2015;73:123–35. https://doi.org/10.1016/j.cemconres.2015.03.008.
[32] Yu Tong L, Xiong QX, Zhang Z, Chen X, Ye G, Feng Liu Q. A novel lattice model to predict chloride diffusion coefficient of unsaturated cementitious materials based on multi-typed pore structure characteristics. Cem Concr Res 2024. https://doi.org/10.1016/j.cemconres.2023.107351.
[33] Zhou Y, Aydin BB, Zhang F, Hendriks MAN, Yang Y. A lattice modelling framework for fracture-induced acoustic emission wave propagation in concrete. Engng Fract Mech 2024;312:110589. https://doi.org/10.1016/j.engfracmech.2024.110589.
[34] Jiang N, Ge Z, Wang Z, Gao T, Zhang H, Ling Y, et al. Size effect on compressive strength of foamed concrete: Experimental and numerical studies. Mater Des 2024. https://doi.org/10.1016/j.matdes.2024.112841.
[35] Mustafa S, Singh S, Hordijk D, Schlangen E, Luković M. Experimental and numerical investigation on the role of interface for crack-width control of hybrid SHCC concrete beams. Engng Struct 2022;251:113378. https://doi.org/10.1016/j.engstruct.2021.113378.
[36] Gu D, Mustafa S, Pan J, Luković M. Reinforcement-concrete bond in discrete modeling of structural concrete. Comput Civ Infrastruct Eng 2023;38:1324–45. https://doi.org/10.1111/mice.12937.
[37] He S, Mustafa S, Chang Z, Liang M, Schlangen E, Luković M. Ultra-thin Strain Hardening Cementitious Composite (SHCC) layer in reinforced concrete cover zone for crack width control. Engng Struct 2023. https://doi.org/10.1016/j.engstruct.2023.116584.
[38] Zhang H, Šavija B, Figueiredo SC, Schlangen E. Experimentally validated multi-scale modelling scheme of deformation and fracture of cement paste. Cem Concr Res 2017;102:175–86. https://doi.org/10.1016/j.cemconres.2017.09.011.
[39] Qian Z, Schlangen E, Ye G, van Breugel K. Modeling framework for fracture in multiscale scement-based material structures. Materials (Basel) 2017;10. https://doi.org/10.3390/ma10060587.
[40] Lee DT, Schachter BJ. Two algorithms for constructing a Delaunay triangulation. Int J Comput Inf Sci 1980. https://doi.org/10.1007/BF00977785.
[41] Jiang N, Zhang H, Chang Z, Schlangen E, Ge Z, Šavija B. Discrete lattice fracture modelling of hydrated cement paste under uniaxial compression at micro-scale. Constr Build Mater 2020;263. https://doi.org/10.1016/j.conbuildmat.2020.120153.
[42] Tepfers R. Cracking of concrete cover along anchored deformed reinforcing bars. Mag Concr Res 1979;31:3–12. https://doi.org/10.1680/macr.1979.31.106.3.
[43] CEB Comite Euro-International Du Beton. CEB-fib Model Code for Concrete Structures 2010. Telford: 2013.
[44] Hamad BS, Seferian ZS. Role of casting position on bond strength of confined tension lap splices in silica fume concrete. Mater Struct 2000;33:584–93. https://doi.org/10.1007/BF02480540.
[45] Goto Y. Cracks formed in concrete around deformed tension bars. ACI J 1971;68(4):244–51. https://doi.org/RFL-03-2009-39-410-1773-035x-101019-200900403.